Highly Efficient Tio2 / Raw Algerian Diatomite And Modified By Phosphoric Acid For Degradation Of Evans Blue Dye And Metronidazole Drug Based On A Solvothermal Process

Rachida Cherrak[1] , Abdelkrim Seghier[2] , Boubekeur Asli[3] , Mohammed Hadjel[4] , Nouredine Benderdouche[5]

[1]Laboratoire des Sciences, Technologie et Génie des Procédés (LSTGP), Université des Sciences et Technologie d'Oran Mohamed Boudiaf USTOMB, BP. 1505 El Menouar, Oran 31000, Algeria. Department of Process Engineering, Faculty of Science and Technology, University of Relizane, Relizane 48000, Algeria. E-mail address: rachidaenv@gmail.com
[2]Laboratory of Environment and Sustainable Development, Faculty of Science and Technology, University of Relizane, 48000, Bourmadia, Algeria
[3]Department of Process Engineering, Faculty of Science and Technology, University of Relizane, Relizane 48000, Algeria.
[4]Laboratoire des Sciences, Technologie et Génie des Procédés (LSTGP), Université des Sciences et Technologie d'Oran Mohamed Boudiaf USTOMB, BP. 1505 El Menouar, Oran 31000, Algeria.
[5]Laboratoire: Structure, Elaboration et Application des Matériaux Moléculaires (SEA2M), Université´ de Mostaganem 27000, Algeria.

Received: 15/01/2025. Accepted: 25/03/2025 Published:15/05/2025

Abstract

This study focuses on the synthesis of a ternary material via a solvothermal process, followed by a calcination route. Spherical TiO2 nanoparticles were immobilized on raw Algerian diatomite, purified with phosphoric acid. The prepared composites were calcined at 300 °C for 2 hours and then were characterized using various techniques. The results revealed that TiO2/diatomite hybrid catalysis exhibited superior distribution over the support surface. Calcined TiO2 raw diatomite (CTRD) and calcined TiO2 phosphoric diatomite (CTPD), the morphology showed a layer of TiO2 anatase deposited on the CTRD surface. The calculated particle sizes of three materials were in the range of 66-80 nm. The photocatalytic degradation of CTPD enhanced degradation of Metronidazole (MTZ) to 99.30% and resulted in 96.25% of Evans Blue dye (EB) degradation. The three composite significantly increased the photocatalytic activity of TiO2, with diatomite effectively hindering the growth of TiO2 grains on its surface.

Keywords: non hydrolytic sol-gel, drug, dye, diatomite, nanoparticles TiO2

1. Graphical abstract

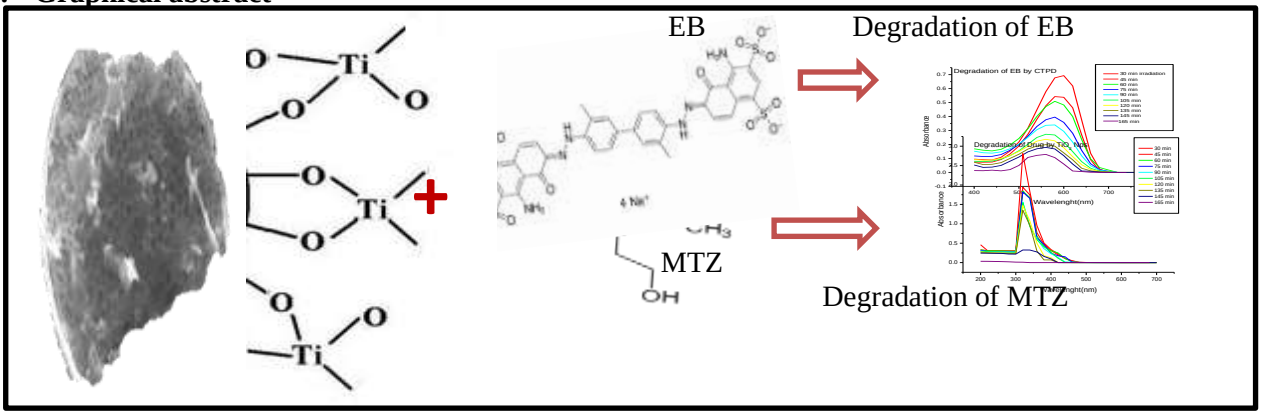

2. INTRODUCTION

In recent years, the degradation of pharmaceutical compounds and synthetic dyes in wastewater has emerged as a critical environmental concern due to their potential adverse effects on ecosystems [1–3] and human health[4,5]. Metronidazole, a commonly used antibiotic [6,7] and Evans Blue, a synthetic dye [8,9] have garnered particular attention due to their persistence and potential ecological impact [10–12]. The discharge of these substances used in various industries into natural aquatic ecosystems poses a significant threat to aquatic life, as traditional wastewater treatment methods may not effectively remove these pollutants, requiring advanced and sustainable treatment technologies to mitigate the environmental impact of these contaminants [13].

Photocatalysis has emerged as a promising approach for the removal of organic pollutants from water [14]due to its eco-friendly nature and high efficiency under irradiation. Titanium dioxide (TiO2), with its well-known photocatalytic properties, has been extensively studied for such applications. However, the practical application of TiO2 nanoparticles faces challenges related to their agglomeration [15–17], their limited surface area, and the difficulty in recovery from treated water.

To address these challenges and enhance the photocatalytic performance of TiO2 [18–22], diatomite, which is a natural, porous, and environmentally friendly material, was selected as a support matrix for TiO2 nanoparticles to prepare a hybrid TiO2/diatomite catalyst.

Nanocomposite materials have good properties such as a more uniform stress distribution throughout the matrix. In recent years, numerous studies have focused on oxide nanoparticles (Fe2O3, Fe3O4 [23,24], Al2O3 [25], ZnO [26–29], SnO2 [27–30], SiO2, TiO2 [31–33], BaTiO3, SrTiO3 [34],Fe –Ce [35],MnO2/NiO [36] ZnO/calcium alumino-silicate[37] .

The non-hydrolytic sol-gel method provides exact control over particle size and shape [38.39], therefore customizing the catalytic characteristics of the resultant composite material.

Nano composites are being studied for their potential to change the matrix's properties or give it new, potentially magnetic properties [40,41].

The objective of this research was to investigate the enhanced photocatalytic activity of the nano-TiO2/Diatomite composite in the degradation of Metronidazole and Evans Blue dye under UV lamp light. This study explored the synergy between the unique properties of TiO2 nanoparticles and the porous structure of diatomite, aiming to improve the degradation efficiency of the composite.

The results contribute significantly to the development of advanced photocatalytic materials for the removal of persistent organic pollutants, thereby providing a sustainable solution to address the environmental challenges associated with pharmaceuticals and synthetic dyes in aquatic ecosystems.

2. EXPERIMENTAL

2.1 MATERIALS

Titanium butoxide Ti (C4H9O)4) 98% (TBOT), absolute ethanol, purity 99.8%, and phosphoric acid, H3PO4 (95.97%) were purchased from Sigma-Aldrich, The reaction was performed at room temperature while stirring under a chemical fume hood due to the large amount of acid fumes in this reaction and diatomite (Kieselghur) was collected in the western region of Algeria .

2.2 METHODS OF CHARACTERIZATION

FTIR spectra were recorded between 400 and 4000 cm-1 using a JASCO 4100 spectrometer. X-ray powder diffraction, XRD patterns were recorded on a Philips diffractometer model PW 1830, with Ni-filtered CuKα (λ= 1.5406 Å) radiation operated at a tube voltage of 40 kV and a tube current of 30 mA. HIROX SH 4000 SEM-EDS BRUKER scanning electron microscope with EDS was utilized to examine the morphology and provide the titane in the produced samples. The sample was fastened with carbon tape to the sample holder. Pollutant absorbance measurements were carried out using a Specord 200 plus UV–vis spectrophotometer.

2.2.1 SYNTHESIS OF TIO2NPS/RAW AND TREATED DIATOMITE COMPOSITES

An economical and straightforward method was used to prepare TiO2/Algerian diatomite nanoparticles composite using the sol-gel and solvothermal techniques. Fig.1 shows the process of synthesizing the nanoparticles composite. In this method, 3 g of raw diatomite was mixed with 10 mL of absolute ethanol.

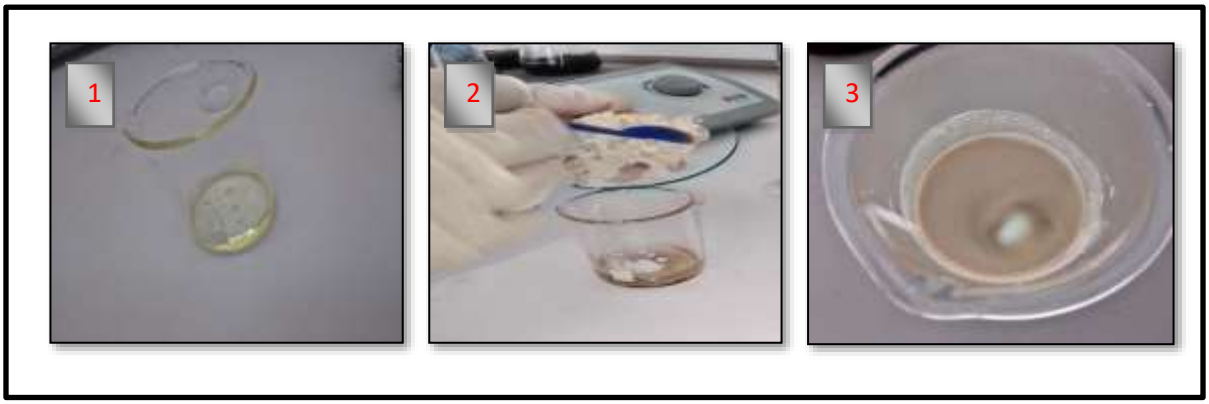

Fig. 1. Steps for synthesis of TiO2/raw and phosphoric acid treated diatomite (1) Titanium butoxide (2) Addition of diatomite (3) Stirring the mixture.

3 mL of titanium butoxide (TBOT) Ti (C4H9O), previously stored in the freezer, was then slowly and carefully added to the initial mixture while vigorously stirring for 15 minutes at room temperature. This process resulted in the formation of a gel. After agitation, the mixture was transferred to a Teflon-lined stainless steel autoclave. The gel was heated at 80°C for 24 hours. The resulting mixture was then calcined at 300°C for 2 hours. The same procedure was repeated for phosphoric acid treated diatomite (CTPD), as well as for the preparation of TiO2 nanoparticles in spherical form in a composite without adding diatomite. Fig. 2 shows pictures of the TiO2 nanoparticles, the calcined TiO2 raw diatomite (CTRD) and the calcined TiO2 phosphoric diatomite (CTPD), respectively. In the diatomite-titanium system, we were able to demonstrate the viability of producing TiO2 nanoparticles by the non-hydrolytic sol-gel approach**[42].** Several tests were conducted to optimize the conditions and obtain nanoparticles material.

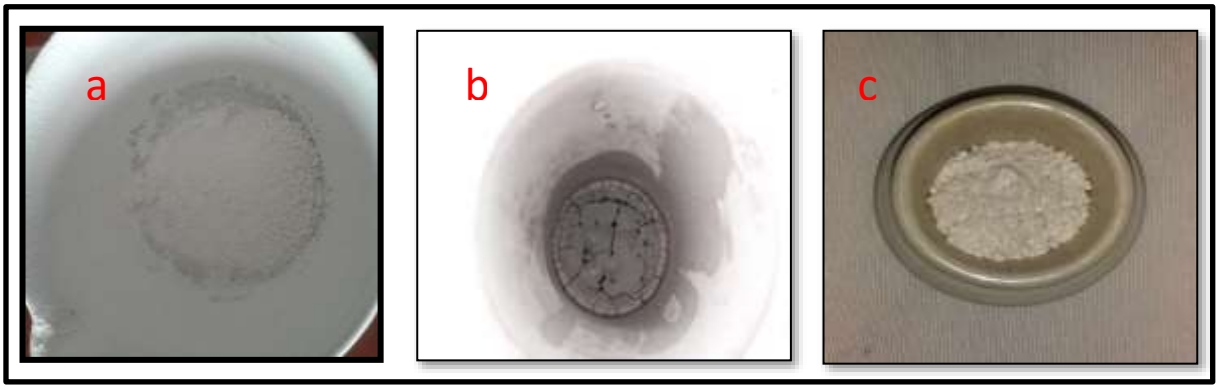

Fig. 2. Materials used (a) TiO2 Nps, (b) CTRD, (c) CTPD, after calcination at 300 °C for 2 hours.

3. RESULTS AND DISCUSSION

3.1 X-RAY DIFFRACTION (XRD) ANALYSIS

The XRD diagrams of TiO2/diatomite composites obtained and the TiO2 nanoparticles are shown in Fig.3. The XRD patterns revealed the presence of three main peaks. The composites CTRD ,CTPD exhibited a broad asymmetric diffraction peak at 2θ = 26.61°, 65.26 °, 64.15°, 26.74°, corresponding to Anatase TiO2. The CTRD also showed a weak quartz diffraction peak. The crystalline size of TiO2 in the composites was calculated Debye–Scherrer equation

$$Dhkl = K \lambda / \beta hkl \, . \cos \theta$$

Where, D is the crystal size of the catalyst, K is dimensionless constant, λ is the X-ray wavelength , β is the full width half maximum (FWHM) of the diffraction peak and θ is the Bragg angle corresponding to (hkl) reflection. The calculated particle sizes of the TiO2 Nps are about 57 nm was successfully deposited on the surface of the raw diatomite , and about 60 nm for the crystallite size of TiO2Nps immobilized on the surface of diatomite purified by phosphoric , indicating that the difference between the supports has

minimal influence on the size of supported TiO2 particles, as Guangxin Zhang et al. [43] observed. Indeed, the diatomite dispersed TiO2 particles and prevented agglomeration, as reported by Zhiming Sun et al. [44] In the realm of photocatalytic degradation, TiO2 has a significant advantage due to its strong photocatalytic activity[45].

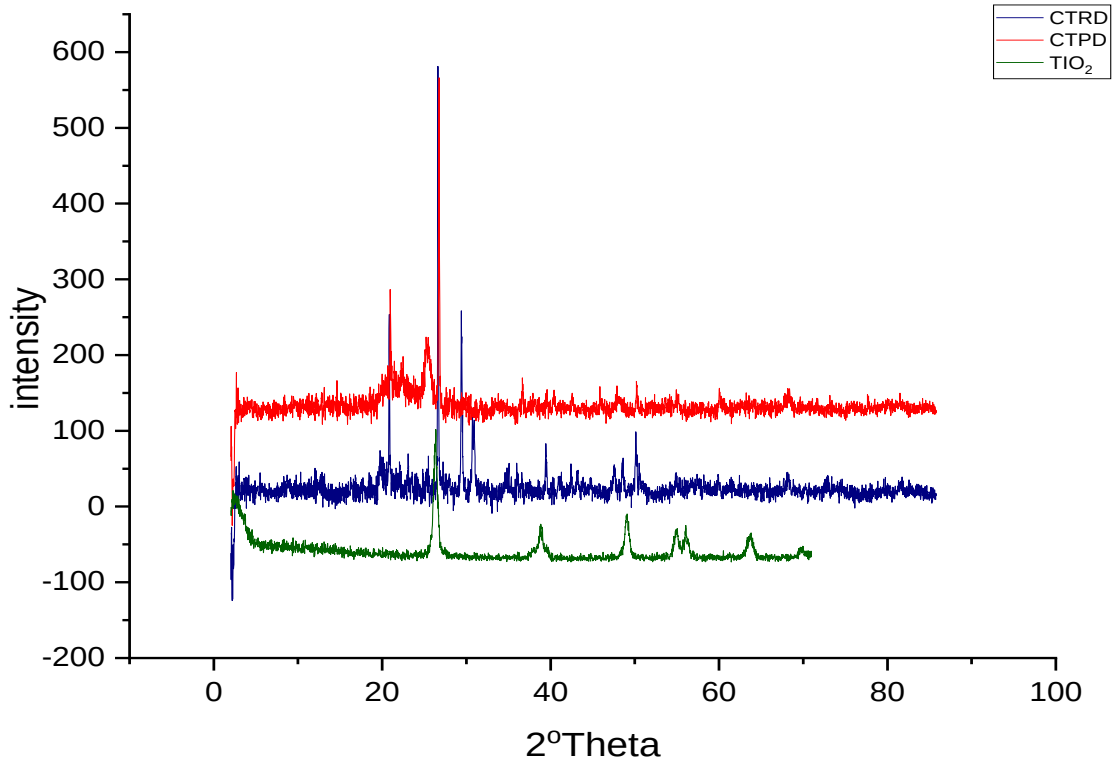

Fig. 3. Powder XRD patterns of CTPD, CTRD and anatase TiO2.

3.2 SCANNING ELECTRON MICROSCOPY (SEM) AND ENERGY DISPERSIVE SPECTRUM (EDS) ANALYSIS

Fig. 4 shows the morphologies and EDS spectra of (a) CTRD, (b) pure TiO2, (c) CTPD. The image of pure TiO2 revealed particle grain sizes falling within the range of 10-100 nm, as depicted in Fig. 4(e). Figs. 4(a) and 4(c), those are apparent that pore structures are uniformly distributed on the surface [22], likely enhancing adsorption capacity. The surface exhibits partial masking by impurities, indicating their removal and reduction following acid treatment. SEM images of CTRD and CTPD demonstrate effective immobilization of TiO2 on the diatomite surface, with the anatase TiO2 phase distributed on the surface and formed a thin layer contributing to enhanced photocatalytic activity. Electron dispersive X-ray spectrometry (EDS) verified the composition of pure CTRD, CTPD, and TiO2 samples, with surface area analysis results presented in Fig. 4(d), Fig. 4(e), and Fig. 4(f), respectively. Characteristic peaks for Si, O, are evident in Fig. 4(d), suggesting that the primary component of CTRD and CTPD is SiO2. Comparatively, characteristic peaks for Ti, consistent with XRD analysis findings, are also observed in the EDS spectrum of TiO2[46].

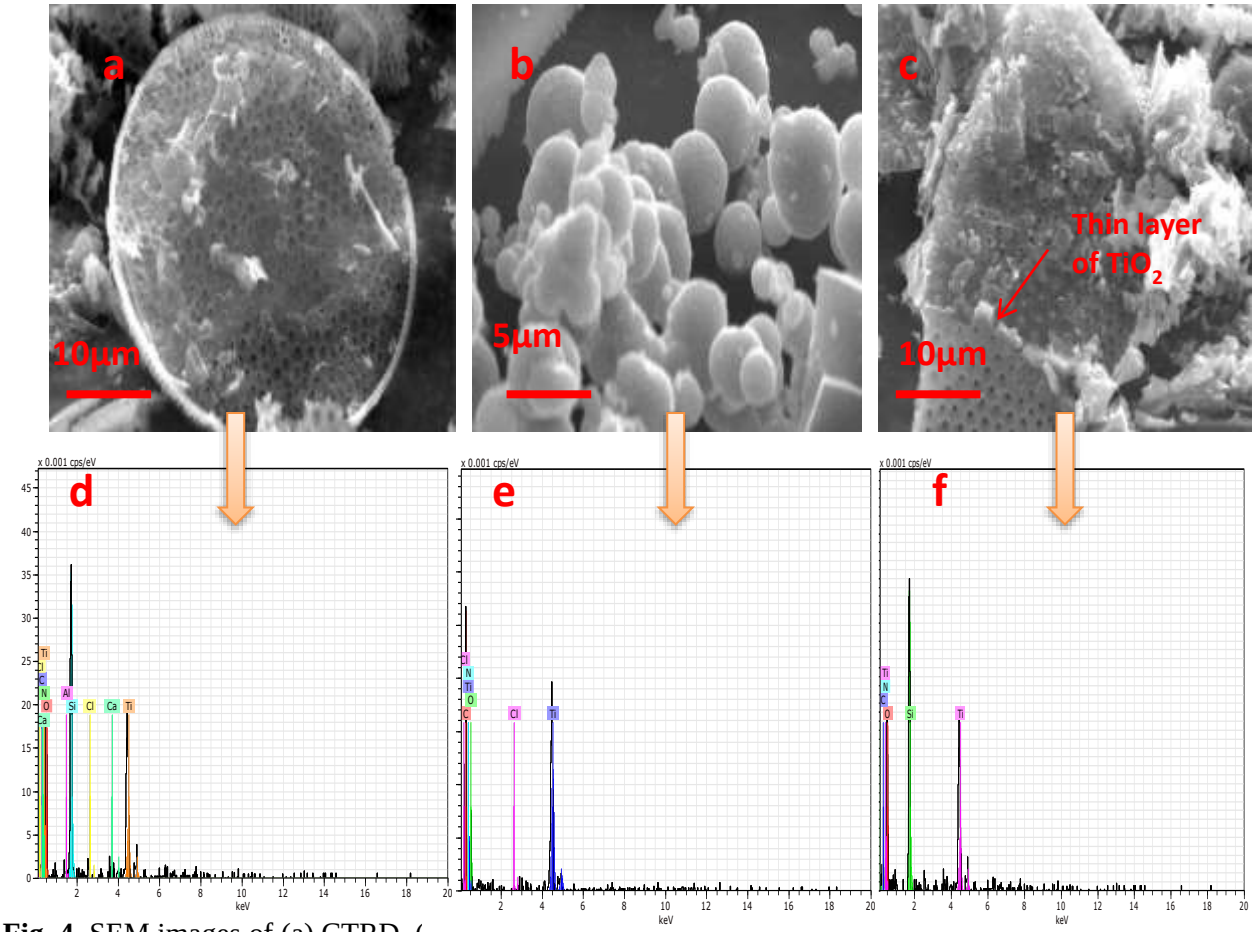

Fig. 4. SEM images of (a) CTRD, (b) TiO2 Nps(c) CTPD, EDS spectra of (d) CTRD, (e) TiO2 Nps, (f) CTPD.

3.3 ATR-FTR ANALYSIS

Infrared spectra, as shown in Fig.5, display several absorption peaks indicating the characteristic bands of the nanocomposite. The IR results of the CTRD, CTPD, and TiO2 spectra are characterized by the following, the observed infrared peak at 3684 cm-1 can be attributed to the vibrations of hydroxyl (OH) groups. Peaks around 540 cm-1 and 794 cm-1 indicate the presence of the Ti-O-Ti bonds. A vibration mode at a wavenumber between 720 cm-1, 1067 cm-1 and corresponds to the vibrations of Si-O-Si bonds present in the CTRD and CTPD composites. The appearance of a broad band, observed at 520 cm-1 and small band around 920 cm-1 corresponding to the Si-O-Ti bond, can be assigned to the characteristic stretching vibration of TiO2 [47,48].

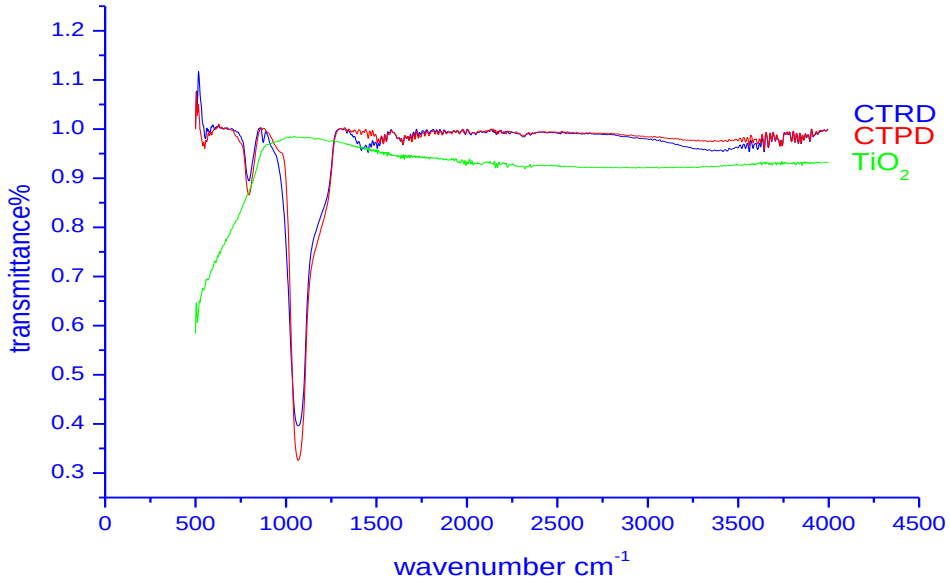

Fig. 5. FT-IR spectroscopy of TiO2/diatomite composites.

4. PHOTOCATALYTIC PERFORMANCE OF CTRD, CTPD AND TIO2

The photolytic performance of the prepared catalysts (CTRD, CTPD) and that of TiO2 nanoparticles was assessed using Evans Blue dye and Metronidazole drug under UV-radiation. The most part, the heterogeneous catalytic process as described by the Langmuir–Hinshelwood (LH) kinetic equation [49] was utilized.

$$r = \frac{dC}{dt} = \frac{K_t K C}{1+KC} \quad (1)$$

Where K is the adsorption rate constant, r is the rate of reaction that varies with time (t), and kr is the reaction rate constant. When t = 0, C = C0, the rate expression based on LH expression can be inferred to first-order kinetics and was explained as follows:

$$-\ln\frac{C}{C_0} = K_{app} t \quad (2)$$

Where t is the reaction time, C is the drug and EB dye concentration in aqueous solution at any given time during photocatalytic degradation, the apparent reaction rate constant (kapp) was used in this investigation as a benchmark to compare the photocatalytic activities of the examined materials.

4.1. EVANS BLUE DYE

Fig.6 shows the absorbance spectra of a 25 mg/L Evans Blue solution λmax = 607 nm as a function of UV-radiation time. Between 0 and 30 minutes, the composites were obscured to observe the effect of adsorption. After 30 minutes, we turned on the UV light and started the photodegradation process It can be seen that discoloration by CTRD gradually increases as a function of radiation time, passing from absorbance 0.303 at the beginning of exposure to UV to 0.02 after 165 min, corresponding to 97.09% degradation whereas for CTPD, a percent degradation of 96.25% was reached within 165 min exposure time, which clearly denotes the better performance [46] of the former with respect to both CTPD and TiO2 where degradation attained 77.12% only. The TiO2 has a significant advantage due to its strong photocatalytic activity, and in the presence of diatomite as support. The dye-composite's contact surface area increases, resulting in better degradation [50].

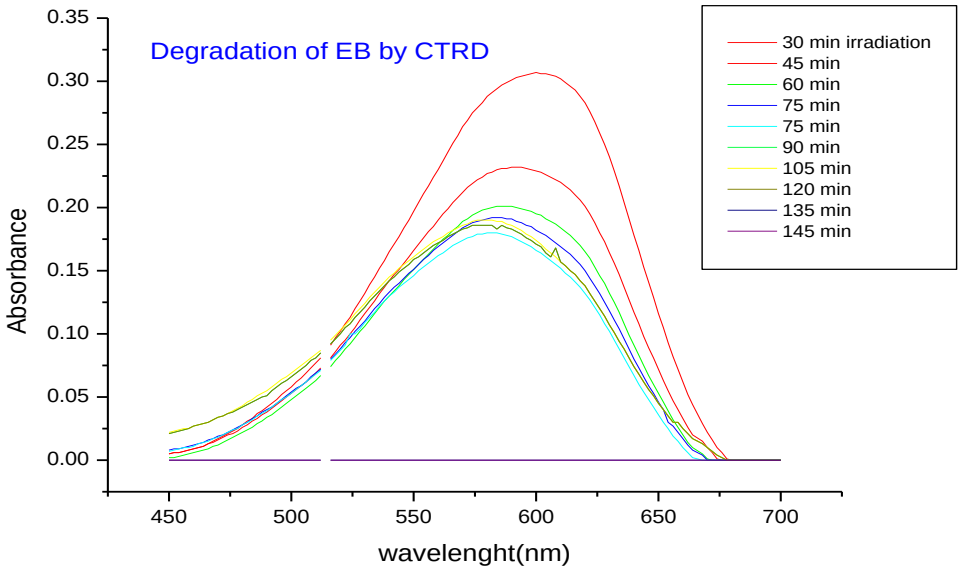

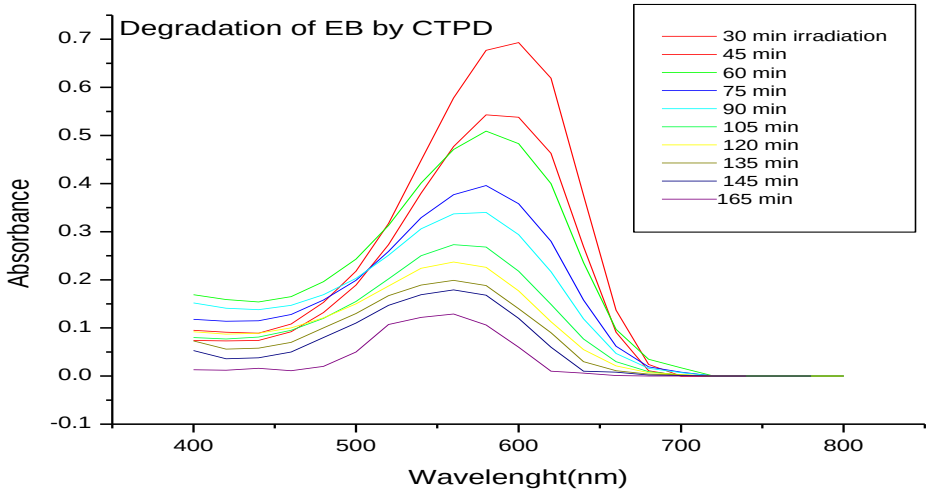

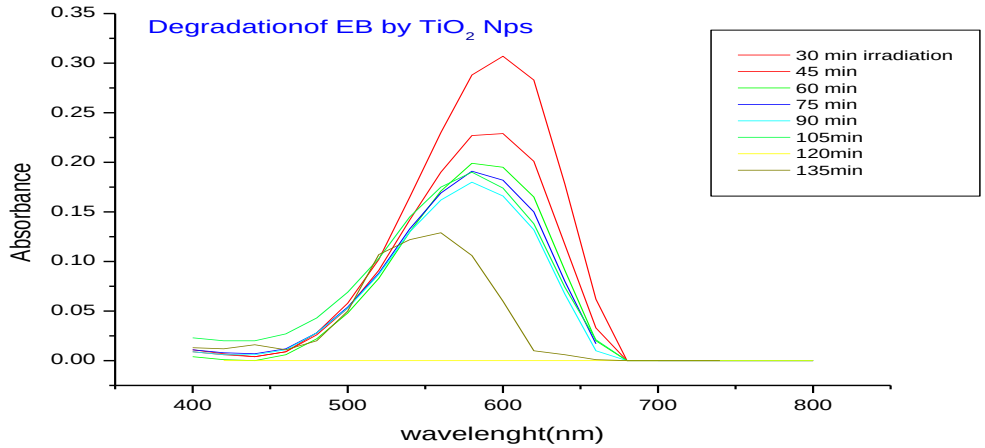

Fig. 6. Photocatalytic degradation kinetics of a 25 mg/L Evans Blue solution (λmax = 607 nm) at different UV-radiation times

Fig. 7 shows the kinetics of photocatalytic degradation of Evans blue dye under UV radiation for TiO2Nps, CTRD and CTPD after the mixtures were kept in the dark for 30 minutes. The nonlinear parameters are shown in Table 1. Pseudo first order reaction rate was obtained for the three materials investigated. Table 2 reports the results obtained in this study in comparison of results published elsewhere [51-54]. Degradation rates obtained with CTRD and CTPD were significantly high and approached those reported in References [52] and [53].

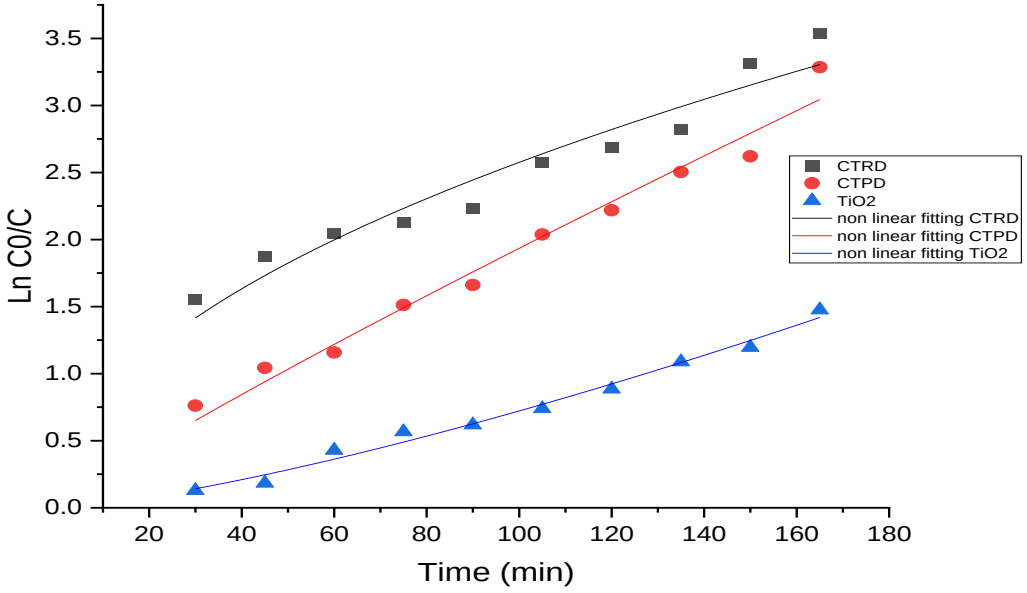

Fig. 7. Kinetics of photocatalytic degradation of Evans Blue dye under UV-light irradiation for TiO2Nps, CTRD and CTPD samples after a contact time of 30 minutes in the dark. Nonlinear fit.

Table 1: Results of UV-light photocatalytic kinetic parameters over TiO2NPs, CTRD and CTPD composites.

Samples	Kapp (10-2)	R2	Reaction order
CTRD	0.005	0.92768	1st
CTPD	0.007	0.97428	1st
TiO2	0.004	0.98495	1st

Table 2: Comparison of photodegradation results of Evans blue with other published experimental results

Samples	Degradation rate (%)	References
TiO2	92	[51]
Fe (II) doped CdS	98.75	[52]
ZnFe2O4	98.83	[53]
CdS-TiO2	84	[54]
TiO2NPs	77.12	Current work
CTRD	97.08	Current work
CTPD	96.25	Current work

4.1.1 DEGRADATION MECHANISM OF EVANS BLUE

Fig. 8 show a mechanism of degradation of Evans blue based on mass spectral analysis as proposed in Reference 55.

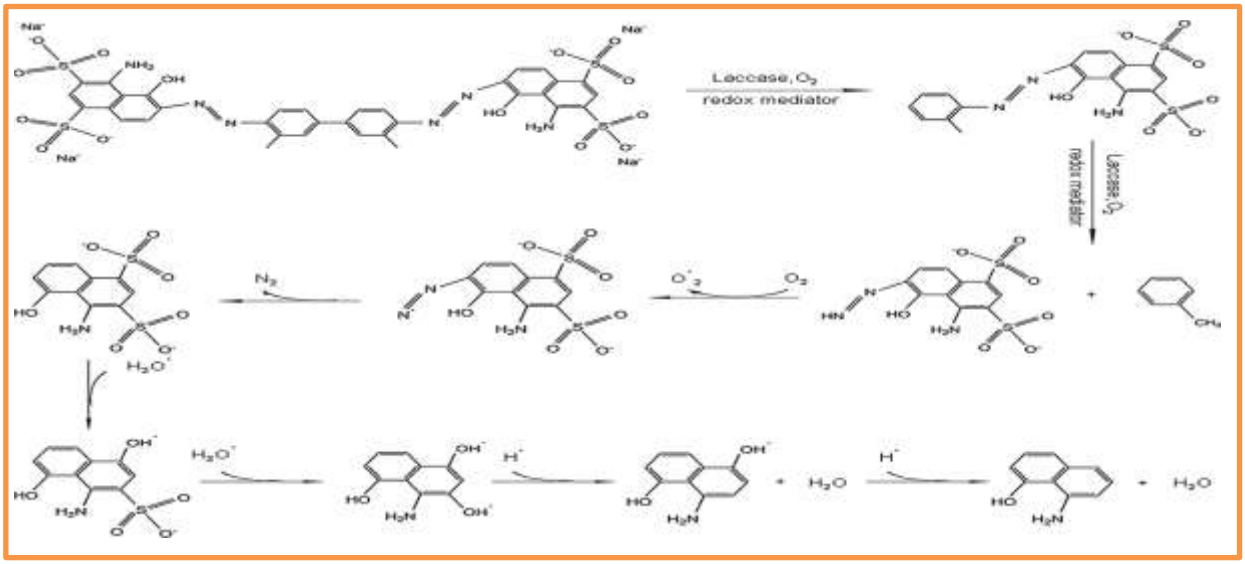

Fig.8. Proposed mechanism for Evans blue degradation by GWLF based on mass spectral analysis [55]

.

4.2. METRONIDAZOLE DRUG

Similarly, Fig. 9 shows the photodegradation of metronidazole at different radiation times through absorbance reduction measurements. Table 3 shows that the photodegradation reaction rate was of pseudo first order with regression coefficients approaching unity.

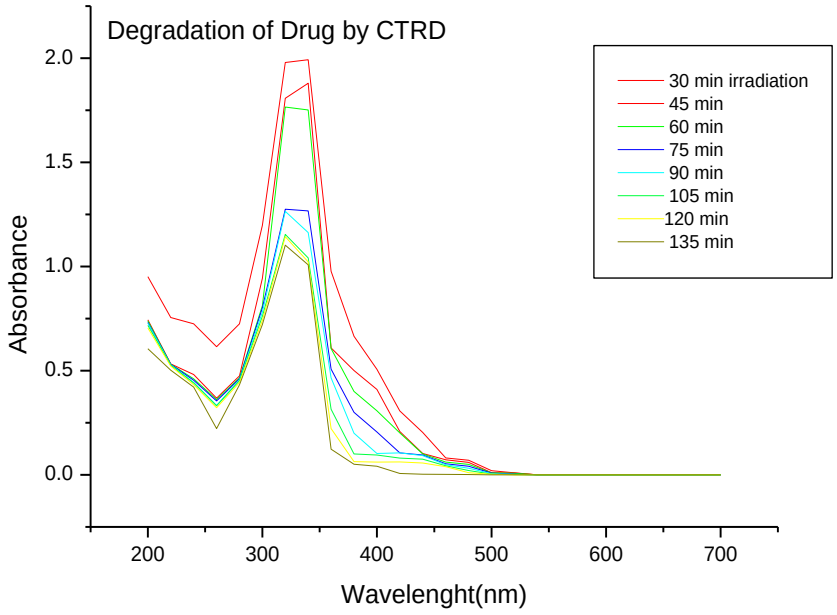

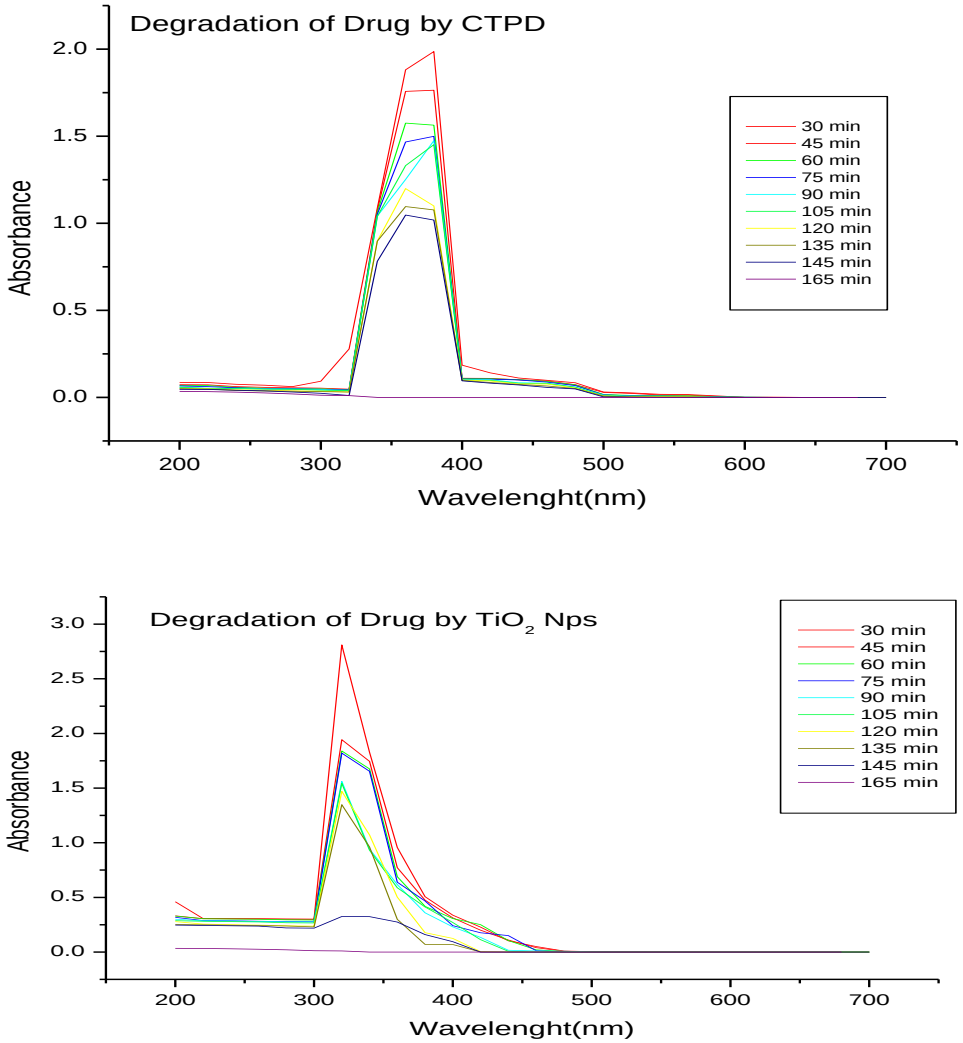

Fig. 9. Kinetic photodegradation of metronidazole drug [25mg/L], (λ max = 320 nm) at different radiation times

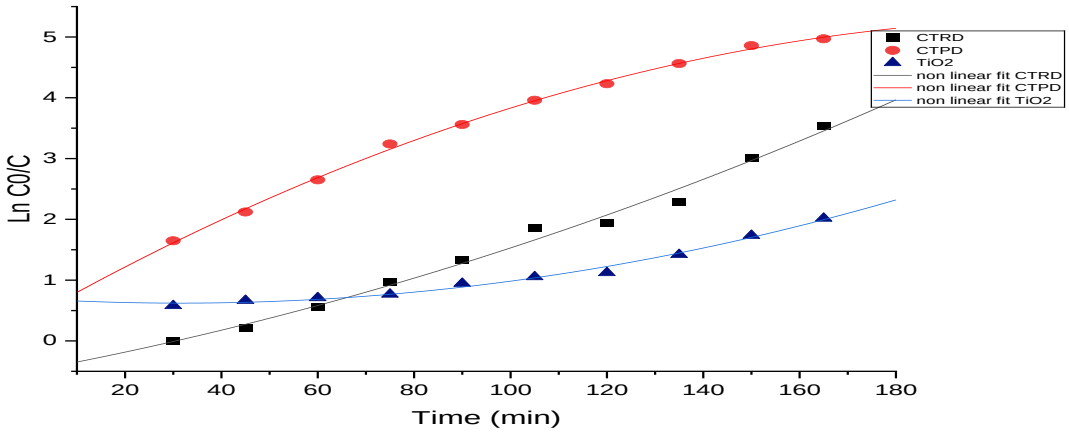

Fig. 10. Kinetics of photocatalytic degradation of metronidazole drug under UV-light irradiation for TiO2Nps, CTRD and CTPD samples after a contact time of 30 minutes in the dark. Nonlinear fit.

Table 3: Results of adsorption and UV-light photocatalytic kinetic parameters over TiO2NPs, CTRD and CTPD composites.

Samples	Kapp (10-2)	R2	Reaction order
CTRD	0.004	0.98734	1st
CTPD	0.013	1	1st
TiO2	0.002	0.99207	1st

The findings reveal that all catalysts exhibited notable photocatalytic activity in degrading dye under visible light irradiation. Notably, the CTRD catalyst demonstrated the highest degradation rate, followed by CTPD and TiO2 Nps, suggesting that the presence of Si-OH groups on diatomite conferred a negative surface charge, thereby enhancing the catalyst's affinity for Evans Blue dye compared to TiO2 alone. Despite composite catalysts utilizing raw diatomite as carriers possessing a higher specific area, their yield was lower than that of TiO2 and CTPD, implying a superior adsorption capacity for the latter. Furthermore, the presence of impurities in raw diatomite may lead to TiO2 nanoparticles deactivation due to aggregation caused by high surface energy.

This study elucidates that the photo degradation of Evans Blue dye and Metronidazole drug follows pseudo-first-order kinetics.

The comparison of the phodegradation results obtained in this study with other published data as shown in Table 4, revealed significant photodegradation but lower than those published in References[6] and [56] but higher than that reported in Reference [57].

Table 4: Comparison of present photodegradation results of Metronidazole with other published experimental results

Samples	Degradation rate (%)	time(min)	References
Fe3O4/rGO/TiO2	98	120	[6]
ZnO/UV	96.55	180	[56]
ZnO/rGO	49.3	160	[57]
TiO2NPs	82.34	150	Current work
CTRD	89.77	135	Current work
CTPD	99.31	165	Current work

4.2.1 DEGRADATION MECHANISM OF METRONIDAZOLE

Likewise, Fig.11 reproduces the mechanism of photodegradation of metronidazole reported in [58].

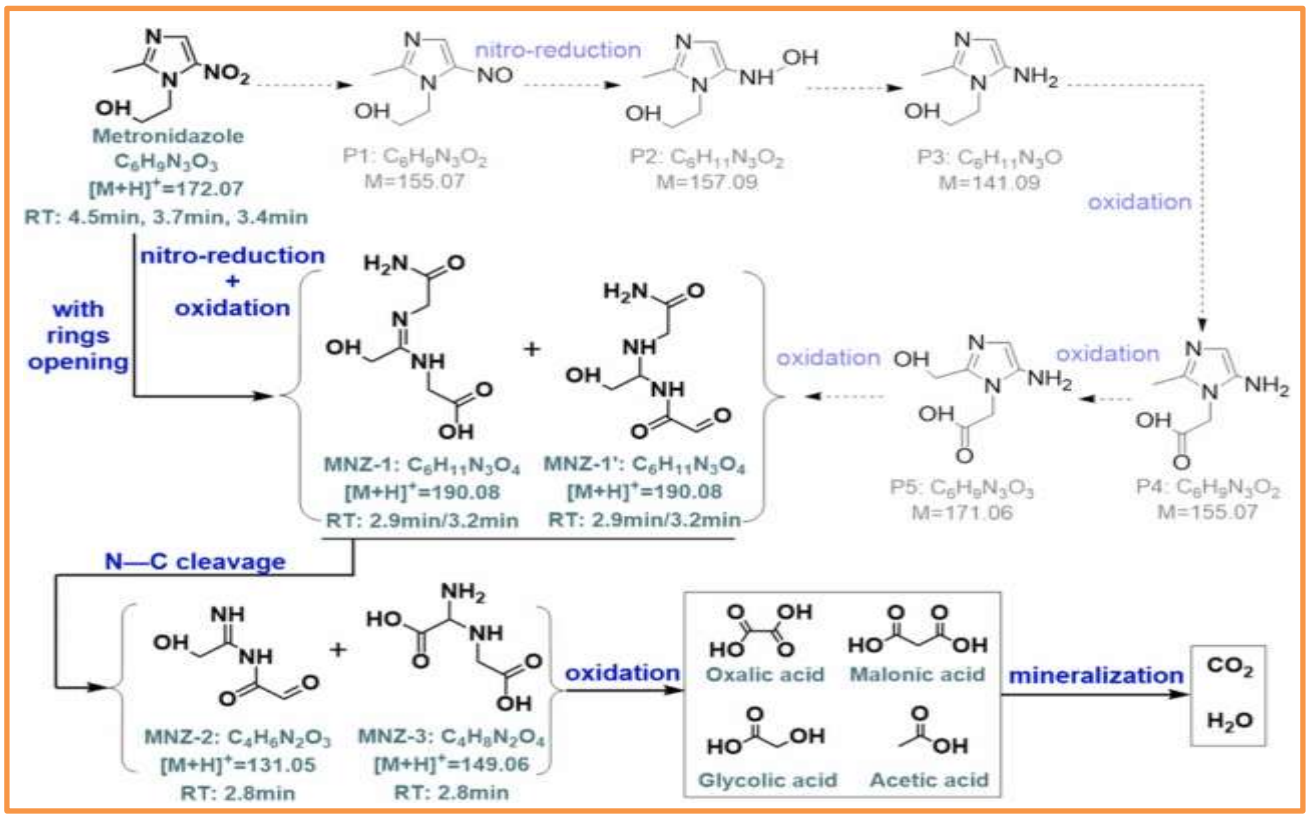

Fig .11. Proposed metronidazole photodegradation under solar light with UiO-66-NH2 photo catalyst: Mechanisms, pathway [58]

The photodegradation of the dye and the drug are depicted in Fig. 12, showing the performance of the treated diatomite with respected to TiO2 nanoparticles.

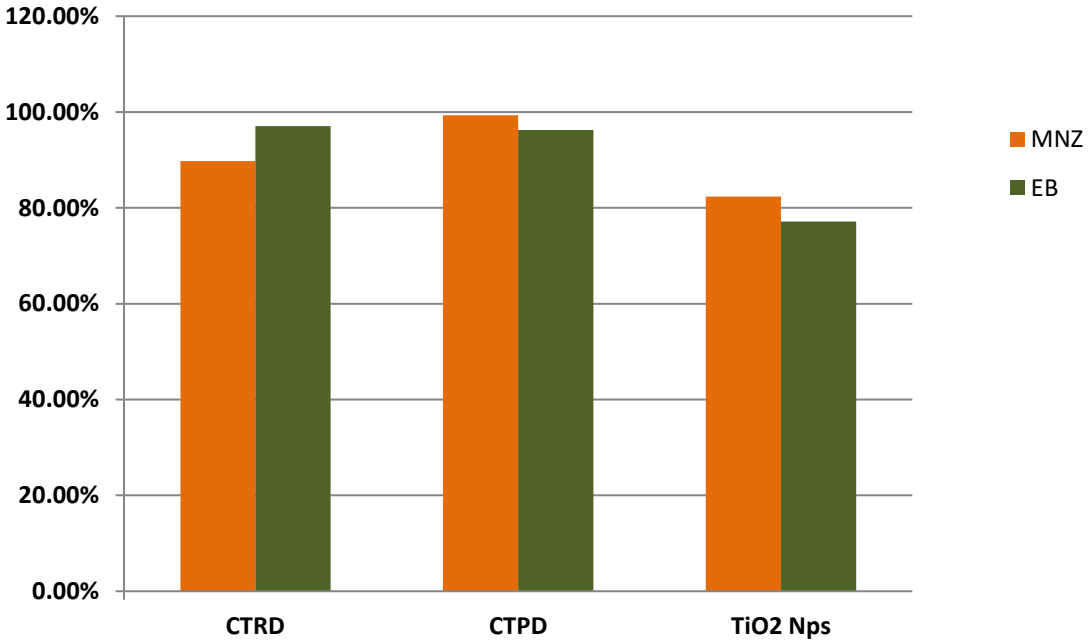

Fig. 12. Histogram of Evans blue dye and Metronidazole drug photodegradation percentage on catalysts CTRD, CTPD and TiO2 NPs

CONCLUSION

Spherical TiO2 nanoparticles were synthesized using a solvothermal method. Titanium tetra-n-butoxide was employed as a precursor, followed by calcination at 300°C for 2 hours. These nanoparticles were

successfully immobilized on the surface of raw diatomite (CTRD). Subsequently, the diatomite was treated with phosphoric acid (CTPD).
The TiO2 nanoparticles are in the anatase phase. X-ray diffraction analysis demonstrated the high crystalline of the TiO2-Nps anatase phase. Using the Scherrer equation, we determined the crystallite sizes of the synthesized composites. For CTRD, a size of approximately 80 nm was obtained, while for CTPD, it was 66 nm
Additionally, scanning electron microscopy (SEM) analysis indicated that the TiO2 particles were uniformly dispersed on the surface of the diatomite. The TiO2 particles formed a layer on the surface of raw diatomite and occupied the pores of diatomite treated with phosphoric acids, as observed in the SEM analysis
The formation of a Si-O-Ti band was observed at around 520.08 cm-1 and 920 cm-1in raw diatomite and approximately 550 cm-1 in treated diatomite, as confirmed by IR analysis.
The photo degradation of Evans Blue dye showed good photocatalytic activity for the catalysts, with a preference for CTRD which degraded 97.088% of the dye after 165 minutes.
The photo degradation of Metronidazole showed good photocatalytic activity for the catalysts, with a preference for CTPD which degraded 99.31% of the drug after 165 minutes, and CTRD degraded 89.77% after 135 minutes at the pH of the solution.

This investigation clarifies that pseudo-first-order kinetics govern the photodegradation of the antibiotic metronidazole and Evans Blue dye.

The photocatalytic activity trend for the three catalysts is as follows CTRD > CTPD> TiO2 for the drug studied, and Evans Blue dye.
These results reveal that the immobilization of titanium on diatomite enhances photocatalytic degradation. CTRD could be a promising catalyst for wastewater treatment due to its excellent photocatalytic properties

REFERENCES

[1] J. Wang, J. Li, C. Jiang, P. Zhou, P. Zhang, J. Yu, The effect of manganese vacancy in birnessite-type MnO2 on room-temperature oxidation of formaldehyde in air, Appl. Catal. B Environ. 204 (2017) 147–155.
[2] L. Zhu, J. Wang, S. Rong, H. Wang, P. Zhang, Cerium modified birnessite-type MnO2 for gaseous formaldehyde oxidation at low temperature, Appl. Catal. B Environ. 211 (2017) 212–221.
[3] S. Huang, W. Wei, L.B. Weschler, T. Salthammer, H. Kan, Z. Bu, Y. Zhang, Indoor formaldehyde concentrations in urban China: preliminary study of some important influencing factors, Sci. Total Environ. 590 (2017) 394–405.
[4] Q. Huang, Y. Hu, Y. Pei, J. Zhang, M. Fu, In situ synthesis of TiO2@ NH2-MIL-125 composites for use in combined adsorption and photocatalytic degradation of formaldehyde, Appl. Catal. B Environ. 259 (2019) 118106.
[5] C.-J. Na, M.-J. Yoo, D.C.W. Tsang, H.W. Kim, K.-H. Kim, High-performance materials for effective sorptive removal of formaldehyde in air, J. Hazard. Mater. 366 (2019) 452–465.
[6] F. Bashiri, S.M. Khezri, R.R. Kalantary, B. Kakavandi, Enhanced photocatalytic degradation of metronidazole by TiO2 decorated on magnetic reduced graphene oxide: Characterization, optimization and reaction mechanism studies, J. Mol. Liq. 314 (2020) 113608.
[7] Z. Bonyadi, F. Noghani, A. Dehghan, J.P. van der Hoek, D.A. Giannakoudakis, S.K. Ghadiri, I. Anastopoulos, M. Sarkhosh, J.C. Colmenares, M. Shams, Biomass-derived porous aminated graphitic nanosheets for removal of the pharmaceutical metronidazole: Optimization of physicochemical features and exploration of process mechanisms, Colloids Surfaces A Physicochem. Eng. Asp. 611 (2021) 125791.
[8] K. Swaminathan, S. Sandhya, A.C. Sophia, K. Pachhade, Y. V Subrahmanyam, Decolorization and degradation of H-acid and other dyes using ferrous–hydrogen peroxide system, Chemosphere. 50 (2003) 619–625.
[9] O. Gulnaz, A. Kaya, F. Matyar, B. Arikan, Sorption of basic dyes from aqueous solution by activated sludge, J. Hazard. Mater. 108 (2004) 183–188.
[10] Y. Fu, T. Viraraghavan, Removal of Congo Red from an aqueous solution by fungus Aspergillus niger, Adv. Environ. Res. 7 (2002) 239–247.
[11] F. Atmani, A. Bensmaili, N.Y. Mezenner, Synthetic textile effluent removal by skin almonds waste, J. Environ. Sci. Technol. 2 (2009) 153–169.
[12] U. Farooq, A.K. Qureshi, M. Farhan, U. Romman, M.E. Khan, W. Ali, A.H. Bashiri, W. Zakri,

Environmentally sustainable fabrication of palladium nanoparticles from the ethanolic crude extract of Oxystelma esculentum towards effective degradation of organic dye, Mater. Today Sustain. 23 (2023) 100463.

[13] C. Hachem, F. Bocquillon, O. Zahraa, M. Bouchy, Decolourization of textile industry wastewater by the photocatalytic degradation process, Dye. Pigment. 49 (2001) 117–125.

[14] N. Liu, X. Chen, J. Zhang, J.W. Schwank, A review on TiO2-based nanotubes synthesized via hydrothermal method: Formation mechanism, structure modification, and photocatalytic applications, Catal. Today. 225 (2014) 34–51.

[15] P.D. Cozzoli, R. Comparelli, E. Fanizza, M.L. Curri, A. Agostiano, Photocatalytic activity of organic-capped anatase TiO2 nanocrystals in homogeneous organic solutions, Mater. Sci. Eng. C. 23 (2003) 707–713.

[16] X. Chen, S.S. Mao, Titanium dioxide nanomaterials: synthesis, properties, modifications, and applications, Chem. Rev. 107 (2007) 2891–2959.

[17] H. Lee, G.M. Kale, Hydrothermal Synthesis and Characterization of Nano-TiO2, Int. J. Appl. Ceram. Technol. 5 (2008) 657–665.

[18] Y. Xia, F. Li, Y. Jiang, M. Xia, B. Xue, Y. Li, Interface actions between TiO2 and porous diatomite on the structure and photocatalytic activity of TiO2-diatomite, Appl. Surf. Sci. 303 (2014) 290–296.

[19] Y. Jia, W. Han, G. Xiong, W. Yang, Layer-by-layer assembly of TiO2 colloids onto diatomite to build hierarchical porous materials, J. Colloid Interface Sci. 323 (2008) 326–331.

[20] X. Meng, Z. Qian, H. Wang, X. Gao, S. Zhang, M. Yang, Sol–gel immobilization of SiO 2/TiO 2 on hydrophobic clay and its removal of methyl orange from water, J. Sol-Gel Sci. Technol. 46 (2008) 195–200.

[21] M.A.M. Khraisheh, Y.S. Al-degs, W.A.M. Mcminn, Remediation of wastewater containing heavy metals using raw and modified diatomite, Chem. Eng. J. 99 (2004) 177–184.

[22] B. Wang, G. Zhang, Z. Sun, S. Zheng, Synthesis of natural porous minerals supported TiO2 nanoparticles and their photocatalytic performance towards Rhodamine B degradation, Powder Technol. 262 (2014) 1–8.

[23] J. Polleux, N. Pinna, M. Antonietti, M. Niederberger, Growth and assembly of crystalline tungsten oxide nanostructures assisted by bioligation, J. Am. Chem. Soc. 127 (2005) 15595–15601.

[24] N. Farooq, R. Luque, M.M. Hessien, A.M. Qureshi, F. Sahiba, M.A. Nazir, A. ur Rehman, A comparative study of cerium-and ytterbium-based GO/g-C3N4/Fe2O3 composites for electrochemical and photocatalytic applications, Appl. Sci. 11 (2021) 9000.

[25] R. Corriu, D. Leclercq, P. Lefevre, P.H. Mutin, A. Vioux, Preparation of monolithic binary oxide gels by a nonhydrolytic sol-gel process, Chem. Mater. 4 (1992) 961–963.

[26] N. Pinna, G. Garnweitner, M. Antonietti, M. Niederberger, A general nonaqueous route to binary metal oxide nanocrystals involving a C− C bond cleavage, J. Am. Chem. Soc. 127 (2005) 5608–5612.

[27] M. Epifani, J. Arbiol, R. Díaz, M.J. Perálvarez, P. Siciliano, J.R. Morante, Synthesis of SnO2 and ZnO colloidal nanocrystals from the decomposition of Tin (II) 2-ethylhexanoate and Zinc (II) 2-ethylhexanoate, Chem. Mater. 17 (2005) 6468–6472.

[28] K.K. Abbas, A.M.H. AbdulkadhimAl-Ghaban, E.H. Rdewi, Synthesis of a novel ZnO/TiO2-nanorod MXene heterostructured nanophotocatalyst for the removal pharmaceutical ceftriaxone sodium from aqueous solution under simulated sunlight, J. Environ. Chem. Eng. 10 (2022) 108111.

[29] K. Shahzad, S. Hussain, M.A. Nazir, M. Jamshaid, A. ur Rehman, A.S. Alkorbi, R. Alsaiari, N.A. Alhemiary, Versatile Ag2O and ZnO nanomaterials fabricated via annealed Ag-PMOS and ZnO-PMOS: An efficient photocatalysis tool for azo dyes, J. Mol. Liq. 356 (2022) 119036.

[30] G. Neri, A. Bonavita, G. Rizzo, S. Galvagno, N. Pinna, M. Niederberger, S. Capone, P. Siciliano, Towards enhanced performances in gas sensing: SnO2 based nanocrystalline oxides application, Sensors Actuators B Chem. 122 (2007) 564–571.

[31] K. Okada, A. Tanaka, S. Hayashi, K. Daimon, N. Otsuka, Porous alumina ceramics by spray-pyrolyzed powder from aluminum sulfate and aluminum nitrate solutions, J. Mater. Res. 9 (1994) 1709–1713.

[32] V. Lafond, P.H. Mutin, A. Vioux, Non-hydrolytic sol–gel routes based on alkyl halide elimination: toward better mixed oxide catalysts and new supports: Application to the preparation of a SiO2–TiO2 epoxidation catalyst, J. Mol. Catal. A Chem. 182 (2002) 81–88.

[33] R. Cherrak, M. Hadjel, N. Benderdouche, Heterogenous photocatalysis treatement of azo dye methyl Orange by nano composite TiO2/diatomite, Orient. J. Chem. 31 (2015) 1611.

[34] M. Niederberger, G. Garnweitner, N. Pinna, M. Antonietti, Nonaqueous and halide-free route to crystalline BaTiO3, SrTiO3, and (Ba, Sr) TiO3 nanoparticles via a mechanism involving C− C bond formation, J. Am. Chem. Soc. 126 (2004) 9120–9126.

[35] Yu Lei a,b, Yixing Hao a, Hao Cheng b, Jianfeng Ma a,*, Yong Qin a, Yong Kong a, Sridhar Komarneni Degradation of Orange II by Fe2O3 and CeO2 nanocomposite when assisted by NaHSO3Colloids and Surfaces A: Physicochemical and Engineering Aspects 628 (2021) 127315

[36]X. Zhang, J. Ma, C. Fan, M. Peng, S. Komarneni, Enhancement of photo-fenton-like degradation of orange II by MnO2/NiO nanocomposite with the synergistic effect from bisulfite, J. Alloy. Compd. 785 (2019) 343–349.

[37]H. P. Shivaraju, K. Byrappa, M. B Shayan, T. Rungnapa, S. Pakamard, V. Kumar, S. Ananda Hydrothermal coating of ZnO onto calcium alumino silicate beads and their application in photodegradation of amaranth dye Materials Research Innovations 14(2010) 73-79 doi.org/10.1179/143307510X12599329343367

[38] C. Legrand-Buscema, C. Malibert, S. Bach, Elaboration and characterization of thin films of TiO2 prepared by sol–gel process, Thin Solid Films. 418 (2002) 79–84.

[39]J. Yu, Y. Zhou, H. Xu Microwave hydrothermal synthesis and photodegradation activities for ciprofloxacin under visible light of InVO4 nanocrystals Materials Research Innovations 18(2014)196
200 .https://doi.org/10.1179/1433075X13Y.0000000186

[40] S. Li, J. Qin, A. Fornara, M. Toprak, M. Muhammed, D.K. Kim, Synthesis and magnetic properties of bulk transparent PMMA/Fe-oxide nanocomposites, Nanotechnology. 20 (2009) 185607.

[41] A.A. Novakova, V.Y. Lanchinskaya, A. V Volkov, T.S. Gendler, T.Y. Kiseleva, M.A. Moskvina, S.B. Zezin, Magnetic properties of polymer nanocomposites containing iron oxide nanoparticles, J. Magn. Magn. Mater. 258 (2003) 354–357.

[42] Mao T, Zha J, Hu Y, Chen Q, Zhang J, Luo X. Research Progress of TiO2 Modification and Photodegradation of Organic Pollutants. Inorganics. 2024; 12(7):178. https://doi.org/10.3390/inorganics12070178

[43] Z.G. Zhang GuangXin, W. Bin Wang Bin, S.Z. Sun ZhiMing, Z.S. Zheng ShuiLin, L.S. Liu ShuShu, A comparative study of different diatomite-supported TiO2 composites and their photocatalytic performance for dye degradation., (2016).

[44] Z. Sun, Z. Hu, Y. Yan, S. Zheng, Effect of preparation conditions on the characteristics and photocatalytic activity of TiO2/purified diatomite composite photocatalysts, Appl. Surf. Sci. 314 (2014) 251–259.

[45] Q. Feng, T. Wang, F. Zhang, B. Song, K. Du Synthesis of TiO2 photocatalytic materials via solid-state reaction and its photodegradation property for methyl orange Materials Research Innovations 18,(2014) S4-92-S4-96 . https://doi.org/10.1179/1432891714Z.000000000650

[46] S. Pal, G. De, A New Approach for the Synthesis of Au− Ag Alloy Nanoparticle Incorporated SiO2 Films, Chem. Mater. 17 (2005) 6161–6166.

[47] Z. Sun, C. Bai, S. Zheng, X. Yang, R.L. Frost, A comparative study of different porous amorphous silica minerals supported TiO2 catalysts, Appl. Catal. A Gen. 458 (2013) 103–110.

[48] M. Epifani, G. De, A. Licciulli, L. Vasanelli, Preparation of uniformly dispersed copper nanocluster doped silica glasses by the sol–gel process, J. Mater. Chem. 11 (2001) 3326–3332.

[49] B. Wang, F.C. de Godoi, Z. Sun, Q. Zeng, S. Zheng, R.L. Frost, Synthesis, characterization and activity of an immobilized photocatalyst: natural porous diatomite supported titania nanoparticles, J. Colloid Interface Sci. 438 (2015) 204–211.

[50]Dasari Ayodhya, Guttena Veerabhadram Ultrasonic synthesis of g-C3N4/CdS composites and their photodegradation, catalytic reduction, antioxidant and antimicrobial studies Materials Research Innovations 24 (2020) 210-228 . https://doi.org/10.1080/14328917.2019.1634356

[51] A. Zolfagharia, M. Riazian, M. Ashjari, Photodegradation of methylene blue and evans blue by iron and sulphur doped TiO2 nanophotocatalyst under ultraviolet and visible light irradiation, J. Mex. Chem. Soc. 65 (2021) 357–375.

[52] M.J. Pawar, A.D. Ingle, V.B. Nimbalkar, R.K. Taywade, Synthesis and characterization of Fe (II) doped CdS nanoparticles and photodegradation of acid blue–29 (AB-29) dye, J. Nanosci. Technol. (2020) 879–881.

[53] F. Gönen, G. Tekinerdoğan, Synthesis of specific ZnF based nanoparticles (ZnFe2O4): antimicrobial properties, surface characteristics, and adsorption activity for AB 29 textile dye, J. Nanotechnol. 2020 (2020) 3139701.

[54] N. Qutub, P. Singh, S. Sabir, S. Sagadevan, W.-C. Oh, Enhanced photocatalytic degradation of Acid Blue dye using CdS/TiO2 nanocomposite, Sci. Rep. 12 (2022) 5759.

[55] J. Xia, Q. Wang, Q. Luo, Y. Chen, X.-R. Liao, Z.-B. Guan, Secretory expression and optimization of Bacillus pumilus CotA-laccase mutant GWLF in Pichia pastoris and its mechanism on Evans blue degradation, Process Biochem. 78 (2019) 33–41.

[56] M. Farzadkia, A. Esrafili, M.A. Baghapour, Y.D. Shahamat, N. Okhovat, Degradation of metronidazole in aqueous solution by nano-ZnO/UV photocatalytic process, Desalin. Water Treat. 52 (2014) 4947–4952.

[57] S. Dong, Y. Li, J. Sun, C. Yu, Y. Li, J. Sun, Facile synthesis of novel ZnO/RGO hybrid nanocomposites with enhanced catalytic performance for visible-light-driven photodegradation of metronidazole, Mater. Chem. Phys. 145 (2014) 357–365.

[58] Y.-L. Wang, A. Gómez-Avilés, S. Zhang, J.J. Rodriguez, J. Bedia, C. Belver, Metronidazole photodegradation under solar light with UiO-66-NH2 photocatalyst: mechanisms, pathway, and toxicity assessment, J. Environ. Chem. Eng. 11 (2023) 109744.